Numerical Analysis of Electron Energy Distribution Function and Its Effects on the H^- Production in Linac4 H^- Source*)

Shintaro MOCHIZUKI, Stefano MATTEI[1)], Kenjiro NISHIDA, Akiyoshi HATAYAMA and Jacques LETTRY[1)]

Faculty of Science and Technology, Keio University, 3-14-1 Hiyoshi, Kohoku-ku, Yokohama 223-8522, Japan
[1)]*CERN, 1211 Geneva 23, Switzerland*

(Received 30 November 2015 / Accepted 2 March 2016)

In order to enhance the H^- surface production in hydrogen negative ion sources, it is important to increase the density of the H atoms dissociated from H_2 molecule and the resultant atomic flux towards the surface of the plasma grid. In this paper, the effect of the Electron Energy Distribution Function (EEDF) on the dissociation of H_2 in Linac4 H^- source has been studied using Electromagnetic Particle In Cell (EM-PIC) simulation with Monte Carlo method for Collision Processes (MCC). It has been shown that the rate coefficient of dissociation reactions can be enhanced in the lower H_2 gas pressure regime, while the H atom production rate becomes larger in the higher pressure regime. It is suggested that the optimal H_2 gas pressure to maximize the H atom production is determined by the balance of rate coefficient and the H_2 density.

Keywords: negative ion source, rf plasma, electron energy distribution function, dissociation rate, particle in cell

DOI: 10.1585/pfr.11.2406044

1. Introduction

In order to understand Radio Frequency Inductively Coupled Plasmas (RF-ICPs) in hydrogen negative ion sources, the numerical simulation code based on the Electromagnetic Particle in Cell (EM-PIC) Model with Monte Carlo method for Collision Processes (MCC) has been developed [1]. This code has been applied to the numerical analyses of the hydrogen negative ions source of Linac4 (see Ref. [2] and below) and improved step-by-step by including various effects, such as i) capacitive component of the electric field [3], ii) Coulomb collision [4] and iii) coupling to the Collisional Radiative (CR) model [5, 6] for the calculation of Balmer emission lines from the source plasmas.

The Large Hadron Collider (LHC) requires an upgrade of its injector complex. Linac4 is a 160 MeV H^- accelerator that is currently being built [7] in order to improve the performance of the accelerator complex. To achieve the requirement, the H^- source of Linac4 is being developed to provide the H^- ion current. H^- ions are produced by surface production due to the H_0 atoms incoming to the cesiated surface of the plasma electrode, and these H_0 atoms are produced by dissociation from H_2 molecules. The dissociation rate of H_2 is determined by the density of H_2, the Electron Energy Distribution Function (EEDF) and the electron density. Thus, the EEDF is one of the key parameters to estimate the amount of H^- produced in the source chamber. It is generally difficult to analyze the EEDF experimentally, therefore numerical simulation plays a key role. However, most of previous studies mentioned above were focused on the macroscopic property of RF-ICPs and detailed discussion of the EEDF in RF-ICPs has not been given so far.

The final goals of our study are as follows; i) to understand the dependence of the EEDF on the RF parameters, ii) to understand the effect of the EEDF on the dissociation rate and production rate of H atoms, iii) to estimate the amount of H^- ions produced by surface production in negative ion sources. In the previous paper [8], we have done the initial study of above items, especially the dependence of the EEDF on the initial H_2 gas pressure has been investigated. In the present paper, focusing the first and second items, we extend the previous study and more systematic investigation has been done.

2. Simulation Model

2.1 Basic equations and model geometry

The EM-PIC MCC model used in the present study is almost the same as that in Ref. [3]. Here, we briefly summarize the basic equations, model geometry and main assumptions. More detailed descriptions have been given in Ref. [4].

The model consists of mainly two modules. One is the two-dimensional (2D) model of RF electromagnetic field produced by the external RF-coil and plasma. We can calculate the electromagnetic fields numerically by solving Maxwell Equations. For simplicity, axial symmetry has been assumed. The Finite Difference Time

author's e-mail: mochizuki@ppl.appi.keio.ac.jp

*) This article is based on the presentation at the 25th International Toki Conference (ITC25).

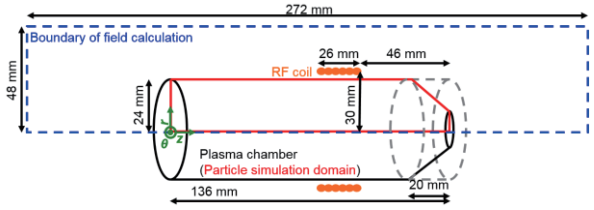

Fig. 1 Model geometry of the numerical simulation.

Domain (FDTD) method [9] has been employed to solve the Maxwell equations. The model of Linac4 H^- source used in this study is shown in Fig. 1. The dimensions of the FDTD domain are taken to be double of that of the plasma chamber, in order to avoid the large reflections at the boundary.

The other part is the particle dynamics model with the three-dimension in the real and velocity space (3D3V). The equations of motion for the charged particles are numerically solved. With the use of the electromagnetic fields calculated by the EM-module mentioned above, the velocity of each charged particle is obtained. The velocity is also changed by collision process. The process is modeled by the MC Null-Collision method [10]. Main collision species taken into account in the simulation are the same as those in Ref. [3]. More than 540 reactions are included. If particles reach the wall, then they are supposed to be absorbed. The motions of plasma particles produce local plasma currents, and these plasma currents are used in the Maxwell equations with the RF-coil current. In this way, we can calculate self-consistently the electromagnetic field and particle dynamics.

2.2 Simulation condition

The numerical time step Δt for the calculation of the electromagnetic field and the particle motion is decided by Courant condition [11] as $\Delta t = 1.0 \times 10^{-12}$ s. The simulation domain is divided into 13056 cells with $\Delta r = \Delta z = 1$ mm. RF coils have been modeled as six independent one-turn coils, and the same RF-coil current flows in each one-turn coil as $I_{\mathrm{RF}}(t) = I_{\mathrm{c}} \sin(\omega_{\mathrm{RF}} t)$. Here I_{c} is the amplitude of the current, $\omega_{\mathrm{RF}} = 2\pi f_{\mathrm{RF}}$ and f_{RF} is the RF driven frequency. In this paper, we set $I_{\mathrm{c}} = 70$ A and $f_{\mathrm{RF}} = 2 \times 10^6$ Hz. The simulation code has been parallelized using Message Passing Interface (MPI) and performed using 128 CPUs.

The initial energy distributions of charged particles are assumed to be Maxwellian distribution with the temperature 0.03 eV. Their initial positions are assumed to distributed uniformly in the chamber, and the initial electron density is taken to be $n_{\mathrm{e}} = 1.0 \times 10^{18}$ m^{-3}, $n_{H_2^+} = 9.0 \times 10^{17}$ m^{-3} and $n_{H^+} = 1.0 \times 10^{17}$ m^{-3} for ions. The density of H_2 is assumed to be uniform in the chamber, the density ratio of the molecules to atoms is set to be $n_{H_2} : n_{\mathrm{H}} = 10 : 1$. The simulations have been performed with various gas pressure: $p_{H_2} = 0.3$, 1, 3, 5, 10 Pa, and n_{H_2} has been determined by p_{H_2} and neutral gas temperature which is assumed to be 300 K.

2.3 Theoretical model of the EEDF

To discuss the validity of the numerical results of EEDFs obtained by the EM-PIC MCC simulation, comparisons will be made with those by a relatively simple analytic approach using Boltzmann equation. Here, we briefly summarize such a simple theoretical model [12] which gives us a basic theoretical guideline to interpret the numerical results of the EEDF in the complex system.

In order to solve the Boltzmann equation of the EEDF analytically, we expand the EEDF f as

$$f = f_0 + f_1, \tag{1}$$

and assume $f_0 \gg f_1$. Here f_0 is the equilibrium component of EEDF and f_1 is the non-equilibrium component. To describe the anisotropy, the vector $\boldsymbol{f}_1$ is introduced. We obtain the following equations from Boltzmann equation,

$$\frac{ne}{3m_{\mathrm{e}}v^2}\frac{\mathrm{d}}{\mathrm{d}v}(v^2\boldsymbol{E}\cdot\boldsymbol{f}_1) = S_0, \tag{2}$$

$$\frac{me\boldsymbol{E}}{m_{\mathrm{e}}}\frac{\mathrm{d}f_0}{\mathrm{d}v} + \frac{e}{m_{\mathrm{e}}}(\boldsymbol{B}\times\boldsymbol{f}_1) = -\boldsymbol{S}_1, \tag{3}$$

where S_0 and $\boldsymbol{S}_1$ are the linearized collision terms. n, e, m_{e}, $\boldsymbol{E}$ and $\boldsymbol{B}$ are the electron density, electron charge, electron mass, electric field and magnetic field, respectively. Here uniform plasma and uniform electric and magnetic fields are assumed.

In the present condition, ω_{RF} is much smaller than cyclotron frequency ω_{c} and collision frequency ν_{m}. This relation is always satisfied thorough one RF cycle. Thus, electromagnetic fields can be assumed to be constant for the collision and cyclotron time scale. We take into account only elastic collision with neutral particles.

Under these conditions, with Eq. (2) and (3), we can obtain f_0 as the Maxwell distribution,

$$f_0 = n\left(\frac{m_{\mathrm{e}}}{2\pi T_{\mathrm{e}}}\right)^{3/2}\exp\left(-\frac{m_{\mathrm{e}}v^2}{2T_{\mathrm{e}}}\right), \tag{4}$$

with the effective temperature

$$T_{\mathrm{e}} = T_{\mathrm{a}} + \frac{2}{3}\frac{e^2E^2}{3m_{\mathrm{e}}\kappa(\omega_{\mathrm{c}}^2+\nu_{\mathrm{m}}^2)}, \tag{5}$$

where T_{a} and κ are the neutral gas temperature and energy transfer coefficient, respectively.

3. Results and Discussions

3.1 Time evolution of electron densities, average energies and typical example of the EEDFs

We have calculated 6 RF cycles that are equal to 3 μs. Figure 2 shows the time evolution of the electron densities and average electron energies for various H_2 gas pressures. As seen from Fig. 2, the electron densities and energies have reach almost steady state in the 6th cycles that

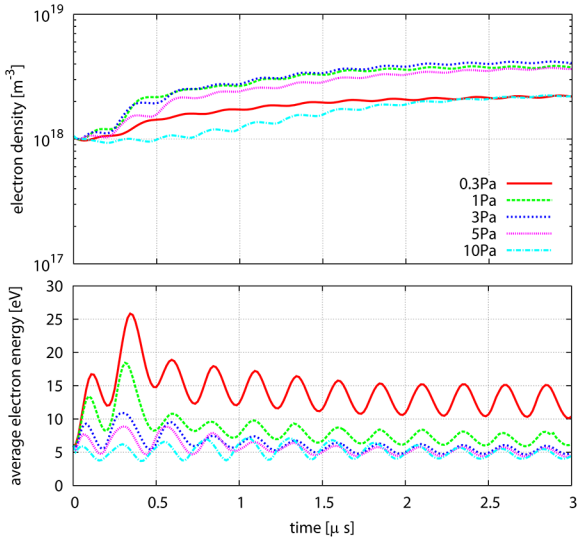

Fig. 2 Time evolution of the electron density (top) and average electron energy (bottom) for various H2 gas pressure.

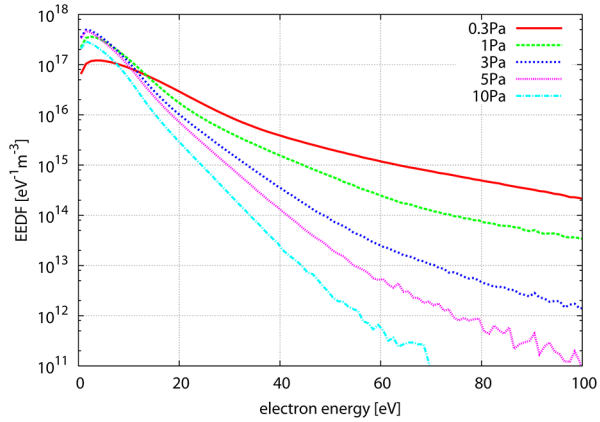

Fig. 3 The EEDFs averaged over the one RF cycle (2.5 ~ 3 μs).

corresponds to 2.5 ~ 3 μs. Therefore, the analysis has been performed based on the results in the 6th cycle.

Figure 3 shows the EEDFs for various gas pressures obtained by simulation. In this figure the EEDFs averaged over the last one RF cycle (i.e., the 6th RF cycle) are shown. It is shown that the low energy components of the EEDFs are relaxed to almost Maxwellian distribution, as indicated by the Eq. (4). It is also shown that the cases with higher pressure have the larger gradients of the EEDF, i.e., the lower electron temperature. This tendency agrees with the Eq. (4) and (5). If H_2 gas pressure increases, the number of the collisions between the electrons and the H_2 molecules increases. The electrons become more likely to loose their energies, therefore the electron temperature becomes low.

In addition, the population of the high energy component of the EEDF, i.e., the non-equilibrium component of the EEDF, is enhanced in the lower H_2 gas pressure regime.

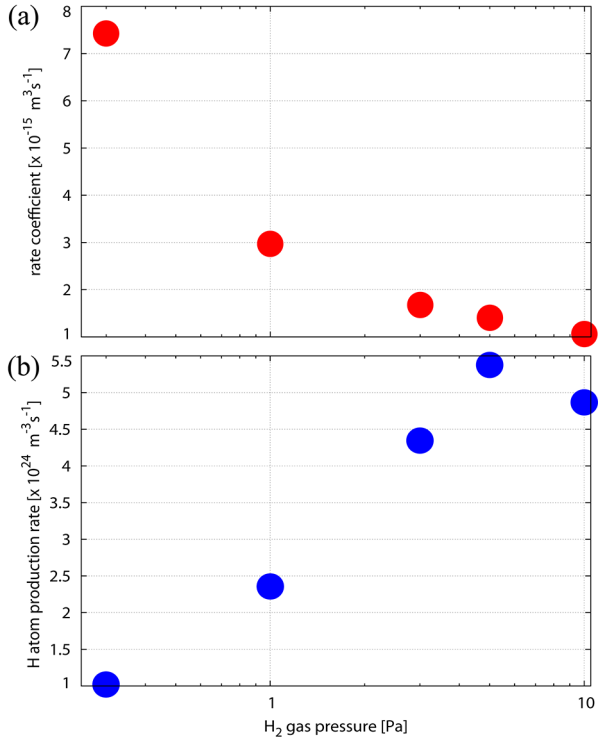

Fig. 4 The dependence of (a) the rate coefficient of the dissociation reactions and (b) H atom production rate on the H_2 gas pressure.

3.2 The relationship between the rate coefficient of the dissociation from H_2 molecule, the H atom production rate and the H_2 gas pressure

H atom is produced by the dissociation reaction of H_2 molecule. The production rate of H atom due to dissociation, S_{diss}, is described as

$$S_{\mathrm{diss}} = \sum_{i=1}^{5} n_{\mathrm{H_2}} n_{\mathrm{e}} \langle \sigma_{\mathrm{i}} v \rangle, \tag{6}$$

where $n_{\mathrm{H_2}}$, n_{e} and σ are the density of H_2, the density of electron and the cross-section of the dissociation reaction, respectively. The symbol i denotes the reaction number. Here five dissociation reactions have been taken into account. They are summarized in Table 1. The symbol $\langle \sigma v \rangle$ is the rate coefficient of the dissociation reactions, K_{diss}, and given as

$$K_{\mathrm{diss}} = \langle \sigma v \rangle = \int \sigma(\varepsilon) v(\varepsilon) f(\varepsilon) \mathrm{d}\varepsilon, \tag{7}$$

where $f(\varepsilon)$ and ε are the electron energy distribution function (EEDF) and the electron energy, respectively.

Substituting the EEDFs obtained by the simulation into Eq. (7), we can estimate K_{diss} and S_{diss} based on these equations. The EEDFs averaged over 1 RF cycle $\overline{f(\varepsilon)}$, that have been shown in Fig. 3, have been used for the analysis.

Figure 4 shows the dependence of the rate coefficient of dissociation K_{diss} and the H atom production rate S_{diss}

Table 1 The dissociation reactions taken into account in the analysis.

Reaction Number	Reactions		Reference
1	$e + H_2(X^1\Sigma_g^+; v = 0) \rightarrow e + H_2(b^3\Sigma_u^+) \rightarrow e + H(1s) + H(1s)$	(H_2 Dissociation 1)	13
2	$e + H_2(X^1\Sigma_g^+) \rightarrow e + H_2^*(1s\sigma_g, nl\lambda\|^1L) \rightarrow e + H(1s) + H^*(2s)$	(H_2 Dissociation 2)	14
3	$e + H_2(X^1\Sigma_g^+) \rightarrow e + H_2^*(2p\sigma_u, nl\lambda\|Q_2\,^1\Pi_u) \rightarrow e + H^*(2s) + H^*(2s)$	(H_2 Dissociation 3)	14
4	$e + H_2(X^1\Sigma_g^+) \rightarrow e + H_2^*(2p\sigma_u; n = 3) \rightarrow e + H(1s) + H^*(n = 3)$	(H_2 Dissociation 4)	14
5	$e + H_2(X^1\Sigma_g^+; v = 0) \rightarrow e + H^+ + H(1s) + e$	(Dissociative Ionization)	14

on H_2 gas pressure for 6th RF cycle. As shown in Fig. 4, K_{diss} is enhanced in the lower pressure condition. This is due to increase in the high energy component of the EEDF (high energy tail) at lower pressure regime. In addition, the dissociation reactions have the large cross-sections in the relatively high energy regime. Therefore, the high energy tail can enhance the amount of dissociation processes, then it leads to the increase in the dissociation rate.

On the other hand, the H atom production becomes larger for the cases with higher gas pressure, in spite of its relatively low rate coefficients. This is because S_{diss} depends not only on the rate coefficient but also on the H_2 gas density. In this calculation isothermal H_2 gas is assumed, therefore the H_2 gas density n_{H_2} is proportional to the H_2 gas pressure p_{H_2}. If we decrease the gas pressure in order to enhance the dissociation rate, the H_2 density must decrease at the same time.

It is indicated that the gas pressure to maximize the production of H atom exists around 5 Pa. The gas pressure to maximize the H atom production is determined by the balance of the rate coefficient and the H_2 gas density. The former has the inverse-proportional dependence and the latter has the proportional dependence on the H_2 gas pressure, therefore it is suggested that the optimal gas pressure to maximize the H atom production exists. The basic tendency of results and conclusion will not differ so much in steady state solution from those obtained in this paper.

3.3 Discussion

In this section, we discuss several uncertainties that exist in the present model and analysis. In order to get more robust conclusion, improvement of the model to remove these uncertainties will be needed.

First, it should be noted that S_{diss} has the dependence on electron density n_e. In this calculation, for the restriction of the simulation cost, all simulations have been started with $n_e = 1.0 \times 10^{18}\,\mathrm{m}^{-3}$, however the way that the electron density build-up from its low-density condition must be different from each gas pressure. The condition to maximize the electron density must be also investigated.

Secondly, in this calculation, the H_2 density is assumed to be constant and distributed uniformly in the chamber. In reality, however, H_2 particles exist non-uniformly in the chamber.

Finally, if a dissociation reaction takes place, then H_2 molecule is depleted in such a region. The effect of the depletion of molecules and transport of neutral particles must be included in the simulation for more accurate estimation and will be future work as well.

4. Conclusion and Outlook

The rate coefficient of the dissociation reactions of H_2 molecule and the production rate of H atom has been estimated using the EEDFs obtained by the numerical simulation. Non-equilibrium characteristics of the EEDF have been taken into account by kinetic EM-PIC simulation. It has been shown that the dissociation rate is enhanced in the lower gas pressure condition because the high energy tail of the EEDF becomes larger. In contrast, the production rate of the H atom becomes smaller in the low pressure because H_2 density decreases. The condition to enhance the H atom production is determined by the balance between the rate coefficient and H_2 gas density.

In order to get the more robust calculation, the improvement discussed in Sec. 3.3 will be necessary in the future. Moreover, in this paper we focused on the dependence of the dissociation rate and production rate on the H_2 gas pressure. However, those two values depend not only on the pressure but also on other parameters, e.g., the input RF power, the RF driven frequency, etc. It is desirable to find the optimal parameters which increase the population of the high energy component of the EEDF without decreasing the H_2 density. The systematic parameter survey for the dependence on the initial and physical parameters will be future work in order to investigate the condition to enhance the H atom production and resultant enhancement of the surface H^- production.

[1] S. Yoshinari, T. Hayami, R. Terasaki, A. Hatayama and A. Fukano, Rev. Sci. Instrum. **81**, 02A728 (2010).
[2] S. Mattei, M. Ohta, A. Hatayama, J. Lettry, Y. Kawamura, M. Yasumoto and C. Schmitzer, AIP Conf. Proc. **1515**, 386 (2013).
[3] S. Mattei, M. Ohta, M. Yasumoto, A. Hatayama, J. Lettry and A. Grudiev, Rev. Sci. Instrum. **85**, 02B115 (2014).
[4] S. Mochizuki, S. Mattei, T. Shibata, K. Nishida, A. Hatayama and J. Lettry, AIP Conf. Proc. **1655**, 020016 (2015).
[5] T. Yamamoto, T. Shibata, M. Ohta, M. Yasumoto, K. Nishida, A. Hatayama, S. Mattei, J. Lettry, K. Sawada and U. Fantz, Rev. Sci. Instrum. **85**, 02B118 (2014).
[6] T. Shibata, S. Mattei, K. Nishida, A. Hatayama and J. Lettry, AIP Conf. Proc. **1655**, 020008 (2015).
[7] J. Lettry, D. Aguglia, J. Alessi, P. Andersson, S. Bertolo, S. Briefi, A. Butterworth, Y. Coutron, A. Dallocchio, N.

David, E. Chaudet, D. Faircloth, U. Fantz, D.A. Fink, M. Garlasche, A. Grudiev, R. Guida, J. Hansen, M. Haase, A. Hatayama, A. Jones, I. Koszar, J.-B. Lallement, A.M. Lombardi, C. Machado, C. Mastrostefano, S. Mathot, S. Mattei, P. Moyret, D. Nisbet, K. Nishida, M. O'Neil, M. Paoluzzi, R. Scrivens, T. Shibata, D. Steyaert, N. Thaus and G. Voulgarakis, Rev. Sci. Instrum. **87**, 02B139 (2016).

[8] S. Mochizuki, S. Mattei, K. Nishida, A. Hatayama and J. Lettry, Rev. Sci. Instrum. **87**, 02B108 (2016).

[9] K. Yee, IEEE Trans. Antennas Propag. **14**, 302 (1966) ISSN 0018-926X.

[10] K. Nanbu, IEEE Trans. Plasma Sci. **28**, 971 (2000).

[11] R. Courant, K. Friedrichs and H. Lewy, Math. Ann. **100**, 32 (1928).

[12] V.E. Golant, A. Zhilinskii and S.A. Sakhavov, *Fundamentals of Plasma Physics* (Wiley, New York, 1977).

[13] P.T. Greenland and D. Reiter, Juelich Report No. JUEL-3528 (1996).

[14] R.K. Janev, D. Reiter and U. Samm, "Collision processes in low-temperature hydrogen plasmas", Juelich Report No. JUEL-4105 (2003).